Three and four identical fermions near the unitary limit

Michael D. Higgins 1 and Chris H. Greene 1,2

¹Department of Physics and Astronomy, Purdue University, West Lafayette, Indiana 47907, USA ²Purdue Quantum Science and Engineering Institute, Purdue University, West Lafayette, Indiana 47907, USA

(Received 9 May 2022; accepted 26 July 2022; published 5 August 2022)

This work analyzes the three and four equal-mass fermionic systems near and at the s- and p-wave unitary limits using hyperspherical methods. The unitary regime addressed here is where the two-body dimer energy is at zero energy. For fermionic systems near the s-wave unitary limit, the hyperradial potentials in the N-body continuum exhibit a universal long-range R^{-3} behavior governed by the s-wave scattering length alone. The implications of this behavior on the low-energy phase shift are discussed. At the p-wave unitary limit, the four-body system is studied through a qualitative look at the structure of the hyperradial potentials at unitarity for the $L^{\pi} = 0^+$ symmetry. A quantitative analysis shows that there are tetramer states in the lowest hyperradial potentials for these systems. Correlations are made between these tetramers and the corresponding trimers in the two-body fragmentation channels. Universal properties related to the four-body recombination process $A + A + A + A \leftrightarrow A_3 + A$ are discussed.

DOI: 10.1103/PhysRevA.106.023304

I. INTRODUCTION

Few-body physics has been extensively studied in a regime where the two-body s-wave interaction is at the unitary limit, i.e., when $a_s \to \infty$. One subset of systems of interest are interacting bosons, which have been studied as a way to probe universality and to understand the manifestations of the three-body Efimov effect [1–3]. Fermionic systems have also been studied extensively in recent years. Some of these studies include interactions of two-component Fermi gases near unitarity, in connection with the Bose-Einstein condensate to Bardeen-Cooper-Schrieffer (BEC-BCS) crossover problem [4–9]. Other works include recent experiments on fermionic atoms, such as ⁴⁰K and ⁶Li, near *p*-wave Feshbach resonances whose interactions are tuned via magnetic fields [10–12].

In a recent study published in Ref. [13], systems consisting of three equal-mass fermions interacting through a Lennard-Jones potential were studied to investigate the role p-wave unitary interactions have on the three-body system, and also to see whether there are signatures of an Efimov effect. As a result of this study, it has become clear that there is no Efimov effect for equal-mass fermionic systems in three dimensions, shown using the Born-Oppenheimer framework. In the hyperspherical Born-Oppenheimer approximation, the equal-mass fermionic system has a lowest potential with a long-range attractive $1/R^2$ tail that resembles an Efimov-like potential. However, when the second-derivative diagonal adiabatic correction is included, the long-range attraction that appears to cause an Efimov effect is canceled, which confirms the nonexistence of the Efimov effect in these systems [14]. Instead there is only one universal trimer state at the *p*-wave unitary limit for symmetries $L^{\pi} = 1^{-}$ and 1^{+} .

One interest in pursuing this work for s-wave interactions near the unitary limit stems from two recent papers [15,16] that investigated low-energy scattering of a few interacting neutrons in the context of few-body nuclear physics. The neutron-neutron scattering length is negative and large compared to the range of the interaction $a/r_0 \sim -19$, thus making few-neutron systems good candidate systems for the study of near-unitary physics. In Ref. [16], as a result of studying low-energy scattering in the N-body continuum for different nuclear interactions, it was found that the long-range form of the Born-Oppenheimer potentials contained a $1/R^3$ term that is universal and only dependent on the scattering length and symmetry. As a result of the long-range form of the potential, this leads to a low-energy enhancement in the density of states that was used to suggest a possible explanation of the 2016 experimental result of Kisamori et al. [17]. These results provide motivation to further look at this type of long-range behavior near the unitary limit for other systems, such as ultracold atomic systems with tunable interactions.

Previous work was able to relate four-body processes and properties to the universal Efimov trimers in the four-boson spectrum [18-23]. In Ref. [18], the four-equal-mass boson system interacting at the s-wave unitary limit was studied in the hyperspherical framework to predict the rate of the four-body recombination process $B + B + B + B \leftrightarrow B_3 + B$, later connected to the Innsbruck experimental data on Cs four-atom recombination in an ultracold quantum gas [20,24]. In particular, the universal ratio of the scattering length $a_c^{(4)}$ where a tetramer becomes bound to the corresponding scattering length $a_c^{(3)}$ for the formation of an Efimov trimer, allowed theory to predict a resonant enhancement in the recombination rate at that scattering length. Other studies addressed interacting bosonic systems at the unitary limit for N > 4[20,22,25-28] to explore universal relations between higher *N*-body bound states and to provide insights into mechanisms for higher *N*-body recombination loss rates.

This article is organized as follows. Section II gives an overview of the theoretical methods used in this work, mainly highlighting features of the Born-Oppenheimer method, as well as giving details on the two-body interactions used. In Secs. III and IV, the main results of this work are presented for both s-wave and p-wave interactions near and at the unitary limit. In Sec. III, the three- and four-body potential energy curves as functions of the hyperradius are analyzed near and at the s-wave unitary limit, where the long-range behavior of the lowest hyperradial potentials are characterized. The implications of the long-range behavior are discussed through an analysis of the elastic phase shift in the three-body and four-body continua. Section IV treats the interactions of four fermions near the s-wave and p-wave unitary limits through analysis of the hyperradial potentials for the 0⁺ symmetry, providing insights into the relation between the universal tetramer states and their correlations with the universal trimer states. Finally, a universal ratio related to trimer and tetramer formation is characterized and shown to provide a useful parameter for future four-body recombination measurements.

II. THEORETICAL METHODS

A. Born-Oppenheimer approach

Here we give an overview of the hyperspherical framework used in this work, which was previously described in Ref. [16]. Within the Born-Oppenheimer approach the three- and four-body systems are solved using an explicitly correlated Gaussian (ECG) basis in conjunction with the hyperspherical framework (CGHS) [8,29–31]. The Hamiltonian for the systems considered here allows for separation of the center-of-mass coordinates from the relative coordinates, i.e., $\hat{H} = \hat{H}_{\text{c.m.}} + \hat{H}_{\text{rel}}$. The center-of-mass Hamiltonian, $\hat{H}_{\text{c.m.}}$, consists only of the kinetic energy operator of the center of mass and will be ignored in the following. The hyperradial and hyperangular kinetic energy operators, along with the particle-particle interactions, are treated in the Hamiltonian of the relative coordinates, \hat{H}_{rel} .

The hyperangular kinetic energy and interaction energy operators together construct the adiabatic Hamiltonian. In hyperspherical coordinates, the generalized *N*-body adiabatic eigenvalue problem needed to be solved is

$$H_{\rm ad}(R,\Omega)\Phi_{\nu}(R,\Omega) = U_{\nu}(R)\Phi_{\nu}(R,\Omega),\tag{1}$$

where R is the hyperradius, Ω is a set of hyperangles, ν is an index that labels the eigenstates $\Phi_{\nu}(R,\Omega)$ of $H_{\rm ad}(R,\Omega)$, $U_{\nu}(R)$ are eigenvalues of $H_{\rm ad}$ at fixed R that represent Born-Oppenheimer potentials, and

$$H_{\text{ad}}(R,\Omega) = \frac{\hbar^2}{2\mu R^2} \left[\Lambda^2 + \frac{(3N-4)(3N-6)}{4} \right] + V_{\text{int}}(R,\Omega), \tag{2}$$

where the operator Λ^2 represents the squared hyperangular grand-angular momentum of the system and $V_{\rm int}(R,\Omega)$ represents the sum of two-body potential operators between the particles. The parameter μ is the hyperradial

reduced mass, defined as $\mu = (m_1 m_2 \cdots m_N / (m_1 + m_2 + \cdots + m_N))^{1/(N-1)}$ [8]. The hyperradius is typically treated as an adiabatic parameter and is defined in general as a coordinate proportional to the square root of the trace of the moment-of-inertia tensor. There is an arbitrariness in the overall scaling of the mass-weighted Jacobi vectors used to construct it, however. Typically in atomic systems, the reduced mass used in the hyperspherical framework is the hyperspherical reduced mass given in Ref. [8]. However, when applying the hyperspherical framework to few-body systems in other fields such as nuclear physics, the reduced mass of choice often used is the nucleon-nucleon two-body reduced mass

The adiabatic Hamiltonian given by Eq. (2) is diagonalized using the CGHS basis. In the noninteracting case, the eigenstates $\Phi_{\nu}(R,\Omega)$ describe the hyperspherical harmonics (HH) with the label ν corresponding to the HH quantum number K (see Ref. [8] and references therein). Furthermore, there is a one-to-one correspondence between the noninteracting eigenstates $\Phi_{\nu}(R,\Omega)$ and the states of a d-dimensional isotropic harmonic oscillator, which helps in understanding why the noninteracting eigenstates exhibit high degeneracies (for an example, see Ref. [32]).

The N-body wavefunction is expanded in the relative coordinates in the eigenstates of Eq. (1), given by the ansatz

$$\Psi_E(R,\Omega) = R^{-\frac{3N-4}{2}} \sum_{\nu'} F_{E,\nu'}(R) \Phi_{\nu'}(R,\Omega).$$
 (3)

The factor (3N-4)(3N-6)/4 in Eq. (2) comes from the multiplying factor of R in Eq. (3), which eliminates the first derivative acting on $F_{E,\nu'}(R)$ in the hyperradial kinetic energy. Computing the quantity $\langle \Phi_{\nu} | \hat{H}_{\rm rel} | \Psi_E \rangle$, where the operation $\langle \cdot \rangle$ indicates integrating over the hyperangular coordinates and tracing over spin degrees of freedom, leads to the following coupled hyperradial Schrödinger equations:

$$\left(-\frac{\hbar^2}{2\mu}\frac{\partial^2}{\partial R^2} + W_{\nu}(R) - E\right) F_{E,\nu}(R)$$

$$-\frac{\hbar^2}{2\mu} \sum_{\nu' \neq \nu} \left(2P_{\nu\nu'}(R)\frac{\partial}{\partial R} + Q_{\nu\nu'}(R)\right) F_{E,\nu'}(R) = 0, \quad (4)$$

where $P_{\nu\nu'}(R) = \langle \Phi_{\nu} | \frac{\partial \Phi_{\nu'}}{\partial R} \rangle$ and $Q_{\nu\nu'}(R) = \langle \Phi_{\nu} | \frac{\partial^2 \Phi_{\nu'}}{\partial R^2} \rangle$ are first- and second-derivative nonadiabatic couplings, and $W_{\nu}(R) = U_{\nu}(R) - \frac{\hbar^2}{2\mu}Q_{\nu\nu}(R)$ is the ν th effective adiabatic potential [33–35].

B. Two-body interactions

The Hamiltonian considered in this work consists entirely of two-body interactions. Throughout, the values of \hbar and m are chosen to be in units where $\hbar=1$ and m=1. Two different types of interactions are used here: either short-range interactions or else a long-range van der Waals interaction with a short-range cutoff. In utilizing the explicitly correlated Gaussian basis, the most convenient form of the interaction is that of a Gaussian interaction or a Gaussian multiplied by some arbitrary power. More explicitly, there are four different

TABLE I. Two-body interaction parameters used for calculations at the s-wave and p-wave unitary limits, where $a_s \simeq -1.0 \times 10^{12} \bar{r}_0$ and $V_p \simeq -1.0 \times 10^{12} \bar{r}_0^3$. The superscript u indicates the quantities are given at the unitary limits.

Interaction	r_0 (units of \bar{r}_0)	α_0^u	r_1 (units of \bar{r}_0)	α_1^u	$r_{\rm eff}$ (units of \bar{r}_0)
		(a) s-way	re (↑↓)		
$V_{(5a)}, n = 0$	1.000000	-2.684005	N/A	N/A	1.435246
$V_{(5a)}, n = 1$	1.750000	-2.853468	N/A	N/A	3.013334
$V_{(5a)}, n=2$	2.000000	-2.444496	N/A	N/A	3.932112
$V_{(5a)}, n=0$	0.100000	-2.684005	N/A	N/A	0.143525
Interaction	r_0 (units of \bar{r}_0)	α_0^u	r_1 (units of \bar{r}_0)	α_1^u	$r_{\rm eff}$ (units of \bar{r}_0^{-1})
		(b) <i>p</i> -way	ve (↑↑)		
$V_{(5a)}, n = 0$	1.000000	-12.09931	N/A	N/A	-2.058647
$V_{(5a)}, n = 1$	1.300000	-12.14525	N/A	N/A	-1.343086
$V_{(5a)}, n=2$	2.000000	-10.02293	N/A	N/A	-0.772240
$V_{(6)}, q = 6, p = 3$	0.995898	16ª	N/A	N/A	-2.080183
$V_{(6)}, p = 6, q = 4$	0.856721	16 ^a	N/A	N/A	-1.957820
	1.000000	26.66253	2.000000	-21.33003	-0.838186
$V^1_{(5b)} \ V^2_{(5b)}$	0.577350	25.88748	0.707107	-34.94809	-2.309161

^aFor $V_{(6)}$, the strength parameter is the C_6 coefficient in Eq. (6) which is set to 16 in units of $E_{\text{vdW}}r_{\text{vdW}}^6$. In this case, $\bar{r}_0 = r_{\text{vdW}}$ and $E_0 = E_{\text{vdW}}$.

types of short-range two-body interactions considered in this work, presented in Eqs. (5):

$$V_n(r) = \alpha_0 \left(\frac{\hbar^2}{2\mu_{2B}r_0^2}\right) (r/r_0)^n e^{-(r/r_0)^2},$$
 (5a)

$$V(r) = \alpha_0 \left(\frac{\hbar^2}{2\mu_{2B}r_0^2}\right) e^{-(r/r_0)^2} + \alpha_1 \left(\frac{\hbar^2}{2\mu_{2B}r_1^2}\right) e^{-(r/r_1)^2},$$
 (5b)

where α_0 and α_1 are dimensionless quantities that define the strength of the interaction, r_0 and r_1 give the range of the interaction, μ_{2B} is the two-body reduced mass, and n defines some arbitrary power. For a given r_0 , the s-wave scattering length and p-wave scattering volume are determined by varying the strength. In this work, the s-wave and p-wave interactions are tuned from noninteracting to the unitary limit, specifically the first poles in the scattering length and scattering volume, just before an s-wave or p-wave two-body bound state forms. Using these two-body interactions, three and four interacting fermionic systems are studied near and at s-wave and p-wave unitary.

A van der Waals interaction with a short-range cutoff is also considered in this work. The general form for this potential used with the ECG basis is given by the expression

$$V(r) = -(C_q/r^q)(1 - e^{-(r/r_0)^2})^p,$$
 (6)

where C_q is the coefficient of the potential tail at large r, q is the power of the potential at large r, and r_0 and p are parameters that control the short-range cutoff. The constraint on the value of p is $2p \geqslant q$ to prevent the interaction from diverging at the origin. To easily evaluate matrix elements, the short-range factor $(1-e^{-(r/r_0)^2})^p$ is expanded using the binomial expansion. From Eq. (6), the behavior of this interaction goes like $-C_q(1/r_0)^{2p}r^{(2p-q)}$ at small r and the behavior goes as $-C_q/r^q$ at large r. The characteristic length scale for this potential is the standard definition $R_q = (1/2)[(2\mu/\hbar^2)C_q]^{1/(q-2)}$ in the limit as $r_0 \to 0$. For the calculations involving Eq. (6), the parameters used are $C_6 =$

16, q = 6, p = 3, and p = 4, with r_0 changing depending on the scattering parameters of interest, namely, the scattering volume for p waves.

From the form of the two-body interactions given in Eqs. (5) and (6), a natural set of length and energy units are \bar{r}_0 and E_0 , where $E_0 = \hbar^2/2\mu_{2\rm B}\bar{r}_0^2$. With these definitions, the values of r_0 and r_1 are in units of \bar{r}_0 and the interaction V(r)is given in units of E_0 by setting $\hbar = 1$ and m = 1, which is the convention used throughout this work for an equal-mass system. With the unit system defined in this way, the problem is recast in a more general way. For a given system, an appropriate choice of \bar{r}_0 and E_0 should be chosen. For example, in atomic systems with van der Waals molecules, a good choice for \bar{r}_0 and E_0 would be the van der Waals length (r_{vdW}) and van der Waals energy (E_{vdW}). The van der Waals length is defined as $r_{\text{vdW}} = (1/2)[(2\mu_{2B}/\hbar^2)C_6]^{1/4}$ and the van der Waals energy is defined as $E_{\text{vdW}} = \hbar^2/2\mu_{2B}r_{\text{vdW}}^2$. Likewise in nuclear systems, \bar{r}_0 and E_0 would have units of fm and MeV. The two-body interactions and their parameters used in this work are given in Table I. The parameters listed are at the unitary limit for the s-wave (first pole in a_s) and p-wave (first pole in V_p) studies described in Secs. III and IV, respectively.

III. INTERACTING FERMIONS NEAR THE S-WAVE UNITARY LIMIT

The first type of few-body systems looked at in this study are the fermionic systems interacting near the s-wave unitary limit, specifically at the first s-wave pole in a_s . This is accomplished by treating two cases: (1) treating the system with definite total angular momentum and parity L^{π} and the spin of the individual particles separately, and (2) treating the system with a definite total angular momentum L and total spin S. Case 1 is emphasized in this work, which is most relevant for experiment. We have computed hyperspherical potential curves for the three- and four-body systems in different spin configurations and total orbital angular momentum using a single Gaussian two-body interaction. The strength of the two-body interaction was tuned to give s-wave scattering lengths

in the range of $-\infty$ to zero. The *s*-wave scattering length dependence of the asymptotic R^{-3} coefficient near *s*-wave unitarity was computed for each symmetry as well as the effective angular momentum $l_{\rm eff}$ controlling the R^{-2} coefficient at unitarity, where at large R, $U_{\nu}(R) \rightarrow \hbar^2 l_{\rm eff} (l_{\rm eff} + 1)/2\mu R^2$. The primary results reported in this section are for a single Gaussian two-body interaction with an interaction range r_0 [see Eq. (5)].

A. Three and four two-component fermions at the s-wave unitary limit

For the first case, the three-body and four-body cases of equal-mass interacting particles are studied in different spin configurations, i.e., $(\uparrow\uparrow\downarrow)$, $(\uparrow\uparrow\downarrow\downarrow)$, and $(\uparrow\uparrow\uparrow\downarrow)$. The $(\uparrow\uparrow\uparrow\uparrow)$ spin configuration is reserved for Sec. IV, which treats p-wave interactions. The two-body interaction between each pair of opposite-spin particles is set to be the same and tuned over a range of large s-wave scattering lengths. Gaussian interactions are used in this analysis, with an interaction range r_0 and strength α_0 , represented by Eq. (5). The strength α_0 is tuned to give different s-wave scattering lengths in the range $0 < |a_s| < \infty$. This work focuses on the region where a_s is negative up to the first pole in a_s . The three-body hyperradial potentials at the s-wave unitary limit are shown in Fig. 1 for $L^{\pi} = 0^+$, 1^- , and 2^+ in the $(\uparrow\uparrow\downarrow)$ spin configuration.

Figure 1 shows the lowest few N=3 hyperradial potential curves for the following symmetries at the s-wave unitary limit: 0^+ , 1^- , and 2^+ symmetry in Figs. 1(a)-1(c), respectively. These potentials shown have been rescaled by $(2\mu/\hbar^2)R^2$ and are shown on a logarithmic scale in R/r_0 . In this representation, the curves approach a constant value at large values of R/r_0 , which represents the effective angular momentum barrier which equals the value of $l_{\text{eff}}(l_{\text{eff}} + 1)$, where $l_{\rm eff}$ is the effective angular momentum quantum number. In the three-body case, the $l_{\rm eff}$ takes on half-integer values for the noninteracting case (i.e., the lowest $l_{\rm eff}$ for the symmetries considered here are 7/2, 5/2, and 7/2 for 0^+ , 1^- , and 2⁺, respectively). When the scattering length and scattering volume are both finite, these same noninteracting values of $l_{\rm eff}$ still apply at large R. At unitarity, however, the value of $l_{\rm eff}$ gets modified to a lower value in some of the channels, indicated by the lower deviations at large R/r_0 in Fig. 1. The reduction of the effective angular momentum barrier has been extensively studied over the years, most notably by Werner and Castin [7] for the three-boson and fermion case, and by Blume and co-workers for the four-fermion case [6,36]. This reduction of the coefficient of R^{-2} in the potential curve at $R \to \infty$ appears to be the same mechanism that reduces the analogous coefficient at unitarity for a system of three bosonic (or different spin fermionic) particles in the famous Efimov effect.

For the four-body case, Figs. 2 and 3 show plots similar to the three-body case discussed previously. These figures display the 0^+ , 1^- , and 2^+ symmetries for the $(\uparrow\uparrow\downarrow\downarrow)$ and $(\uparrow\uparrow\uparrow\downarrow)$ spin configurations, respectively. Like in Fig. 1, these plots show a few of the Born-Oppenheimer potentials plotted versus R/r_0 on a logarithmic scale that highlights the effect of unitarity-limited two-body s-wave interactions on the effective angular momentum barrier in the hyperra-

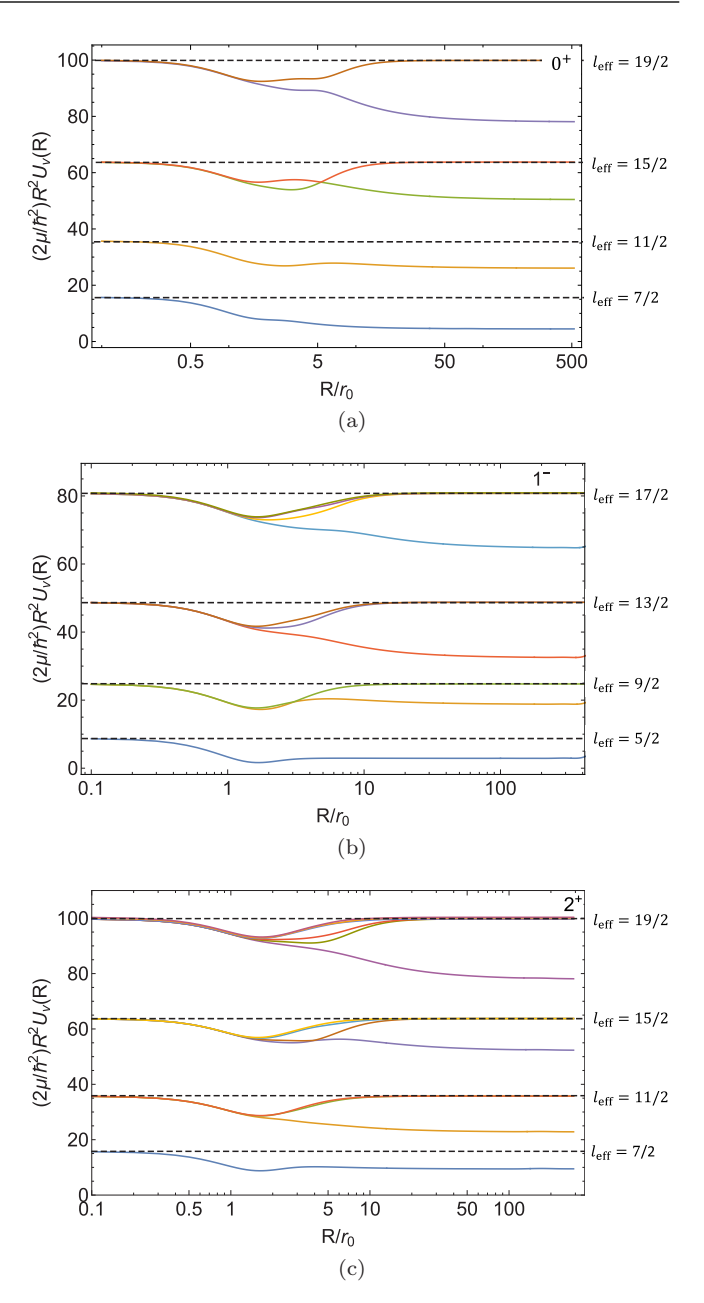


FIG. 1. The lowest few Born-Oppenheimer potential curves for the $(\uparrow\uparrow\downarrow)$ equal-mass three-body system are shown for the symmetries (a) $L^\pi=0^+$, (b) $L^\pi=1^-$, and (c) $L^\pi=2^+$. Each curve represents a different hyperradial potential with channel index ν that increases from the lowest to highest curve. The two-body interactions between all particles are at the first s-wave unitary limit before the formation of an s-wave dimer. The horizontal dashed lines represent the noninteracting rescaled potentials with their effective angular momentum quantum numbers $l_{\rm eff}$ labeled to the right. The hyperradius has been rescaled by the range of the Gaussian interaction r_0 and shown on a logarithmic scale. For some of the higher degenerate channels, the potentials deviate at small hyperradius due to incomplete basis set convergence.

dial equation. For the $(\uparrow\uparrow\downarrow\downarrow)$ spin configuration, the lowest effective angular momentum quantum numbers in the noninteracting limit are $l_{\rm eff}=5$, 6, and 5 for the 0^+ , 1^- , and 2^+ symmetries, respectively. In the $(\uparrow\uparrow\uparrow\downarrow)$ spin configuration,

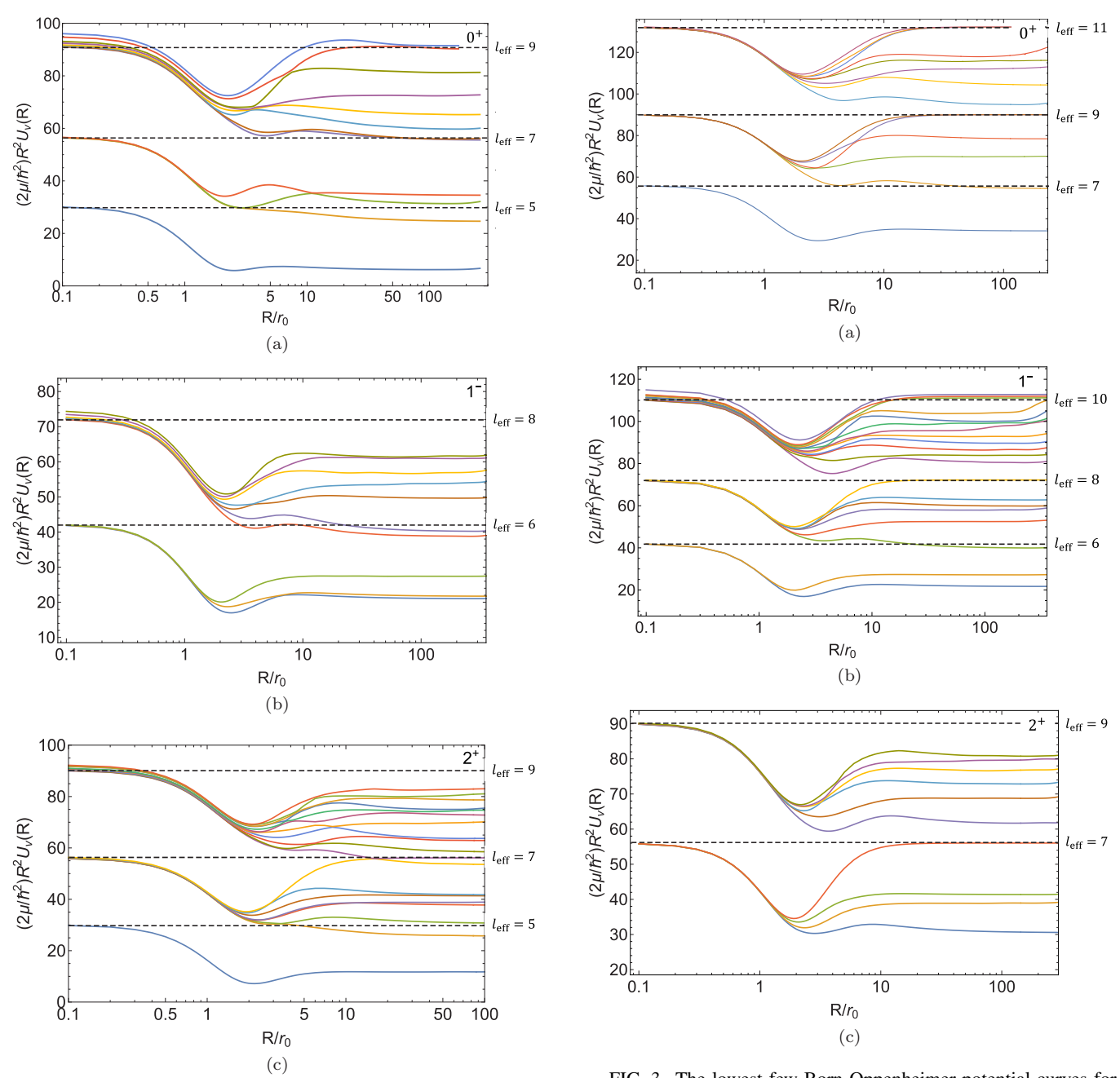


FIG. 2. The lowest few Born-Oppenheimer potential curves for the $(\uparrow\uparrow\downarrow\downarrow)$ equal-mass four-body system are shown for the symmetries (a) $L^{\pi}=0^+$, (b) $L^{\pi}=1^-$, and (c) $L^{\pi}=2^+$. Each curve represents a different hyperradial potential with channel index ν that increases from the lowest to highest curve. The strength of the two-body interaction between all particles is scaled give an infinite s-wave scattering length. The horizontal dashed lines represent the noninteracting rescaled potentials with their effective angular momentum quantum numbers $l_{\rm eff}$ labeled to the right. The hyperradius has been rescaled by the range of the Gaussian interaction r_0 . For some of the higher degenerate channels, the potentials deviate at small hyperradius due to incomplete basis set convergence.

the lowest effective angular momentum quantum numbers are respectively $l_{\rm eff}=7$, 6, and 7 for the 0^+ , 1^- , and 2^+ symmetries. For both symmetries, it should be noted that the lowest noninteracting value of $l_{\rm eff}$ is for the 1^- symmetry among the

FIG. 3. The lowest few Born-Oppenheimer potential curves for the $(\uparrow\uparrow\uparrow\downarrow)$ equal-mass four-body system are shown for the symmetries (a) $L^{\pi}=0^+$, (b) $L^{\pi}=1^-$, and (c) $L^{\pi}=2^+$. Each curve represents a different hyperradial potential with channel index ν that increases from the lowest to highest curve. The strength of the two-body interaction between all particles is scaled give an infinite s-wave scattering length. The horizontal dashed lines represent the noninteracting rescaled potentials with their effective angular momentum quantum numbers $l_{\rm eff}$ labeled to the right. The hyperradius has been rescaled by the range of the Gaussian interaction r_0 . For some of the higher degenerate channels, the potentials deviate at small hyperradius due to incomplete basis set convergence.

ones presented. Since the generalized Wigner threshold law for a squared four-body recombination scattering matrix element is proportional to $k^{2l_{\rm eff}+1}$, one expects the 1^- symmetry to be the dominant recombination symmetry out of these three

parity-favored cases of $(\uparrow\uparrow\uparrow\downarrow)$. In both the three-body and four-body systems, we focus on the hyperradial potentials that go to the modified centrifugal-type barrier at large hyperradius when the particles interact near the unitary limit, where they exhibit universal behavior when tuning the scattering length for $|a_s/r_0| > 10$. This universal behavior manifests in a long-range $1/R^3$ term that depends only on the *s*-wave scattering length and the symmetry of the system.

B. Universal behavior of the hyperradial potentials in the *N*-body continuum

When investigating the *s*-wave behavior in *N*-body systems, an interesting behavior arises in the hyperradial potentials representing the continuum states. Near the unitary regime, the long-range form of some of the continuum channels exhibits a $1/R^3$ behavior. The form of the Born-Oppenheimer potentials representing the *N*-body continuum at large *R* is given by

$$U_{\nu}^{N}(R) \to \frac{\hbar^{2}}{2\mu} \left[\frac{l_{\text{eff}}(l_{\text{eff}}+1)}{R^{2}} + \frac{C_{3,\nu}^{N}}{R^{3}} \right],$$
 (7)

where $l_{\rm eff}$ is the effective angular momentum quantum number, and the coefficient $C^N_{3,\nu}$ is defined as $C^N_{3,\nu}=\mathcal{C}^N_{\nu}a_s$, where a_s is the two-body s-wave scattering length and C_v^N is a universal N-body coefficient that depends on the particle statistics and other quantum numbers of the system. The adiabatic potentials $W_{\nu}(R)$ that include the diagonal nonadiabatic correction $Q_{\nu\nu}(R)$ also follow this same long-range behavior, since the diagonal nonadiabatic correction falls off faster than $1/R^3$. This universal long-range behavior presents itself in the hyperspherical channels whose effective angular momentum quantum number is modified from the noninteracting value at infinite scattering length. The linear dependence of the $1/R^3$ term on the scattering length has been shown for these hyperradial potentials in the continuum for the three-boson system at large scattering length [37,38]. As is shown in what follows, the hyperspherical potentials that approach the noninteracting limit at large R for infinite scattering length do so on a shorter length scale than the potentials that approach the reduced $1/R^2$ coefficient. The coefficient \mathcal{C}^N_{ν} is computed for different total angular momentum states of a given L for various spin configurations, focusing on the three and four identical particle systems with $L^{\pi} = [0^+, 1^-, 2^+]$ in this work.

The spin configurations considered are some total spin states denoted by the total spin quantum number S, and also different individual spin configurations, specifically the $(\uparrow\uparrow\downarrow)$ for the three-body system, and likewise the $(\uparrow\uparrow\downarrow\downarrow)$ and $(\uparrow\uparrow\uparrow\downarrow)$ configurations for the four-particle system. For the treatment of identical particles, the s-wave interaction between the $(\uparrow\downarrow)$ two-body system is tuned from noninteracting to the first s-wave unitary limit, where a low-energy s-wave dimer forms. In some symmetries, tuning the $(\uparrow\uparrow)$ two-body p-wave interaction strength will lead to the formation of a trimer state in the $(\uparrow\uparrow\downarrow)$ configuration.

In this section, the long-range behavior of the lowest few hyperradial potentials in each spin configuration and system size is characterized. Starting with the three-body case for the $(\uparrow\uparrow\downarrow)$ spin configuration, some of the lowest hyperradial potentials have a modified angular momentum barrier at

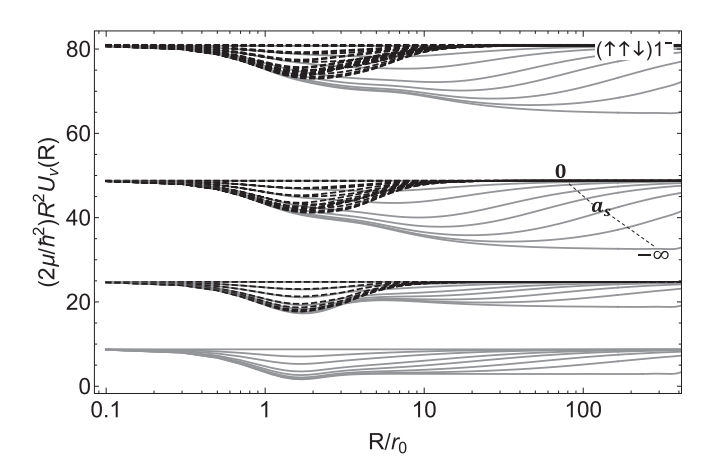


FIG. 4. The lowest few Born-Oppenheimer potential curves for the $(\uparrow \uparrow \downarrow)$ equal-mass three-body system are shown for the 1⁻ symmetry. The solid curves correspond to potentials that exhibit a reduced value of l_{eff} at the unitary limit for large hyperradius, whereas the dashed potentials go to the noninteracting potentials at large hyperradius. The strength of the two-body interactions between all particles is rescaled from the noninteracting limit up to the s-wave unitary limit $(a_s \to -\infty)$. For each set of curves representing a different channel ν , an increase in scattering length on the negative side corresponds to a curve in the set. From highest to lowest, the highest curve is the noninteracting potential, the lowest is the hyperradial potential at the s-wave unitary limit, and a potential in between is for a finite scattering length. The hyperradius has been rescaled by the range of the Gaussian interaction r_0 . The structure of the potential curves for different systems and symmetries is qualitatively similar to the potentials shown here, and thus are not shown.

the *s*-wave unitary limit for all symmetries, which is clearly represented in Fig. 1. For these hyperradial potentials, the long-range behavior of the potential for finite scattering length close to unitarity has the form of Eq. (7). To obtain the symmetry-dependent coefficient C_{ν} , an analysis on the hyperradial potentials is performed at different scattering lengths. In Fig. 4, a subset of hyperradial potentials is shown to illustrate the structure of the long-range behavior at different scattering lengths. The hyperradial potentials for the other systems and symmetries have the same qualitative structure and are not shown here.

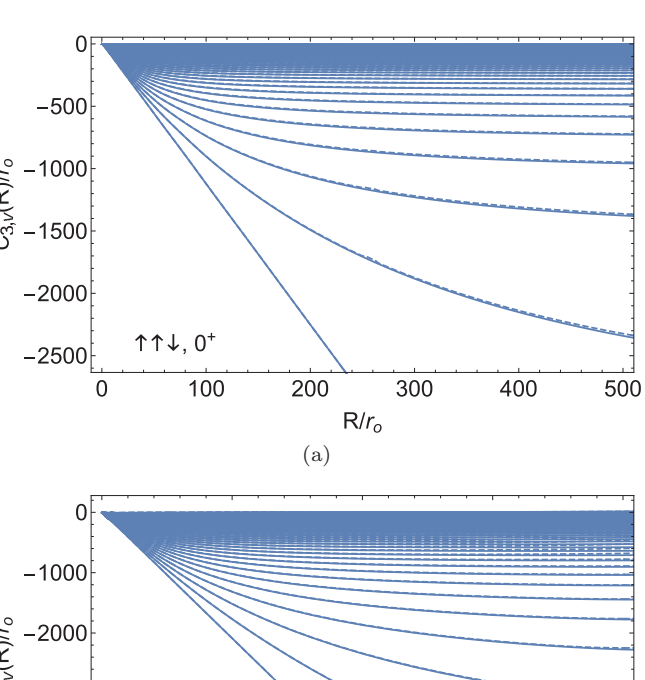
In Fig. 4, the lowest few Born-Oppenheimer potentials are shown to highlight key features that arise when tuning the two-body scattering length from noninteracting to unitarity. As the s-wave scattering length increases on the negative side, some of the potentials start to exhibit a long-range deviation from the noninteracting limit as the angular momentum barrier transitions from the noninteracting value (finite scattering length) to the modified value (infinite scattering length) at large hyperradius. When the hyperradial potentials do not exhibit a modified barrier at infinite scattering length (dashed curves), the deviation from the noninteracting potential appears to be short range. This is visible in Fig. 4 where some of the potentials reach noninteracting behavior already for $R/r_0 \sim 10$ –12. The exact form of the behavior of these potentials (dashed lines) as they start deviating from the noninteracting limit at smaller hyperradius is not studied here, where the focus is on the potentials that go to the reduced

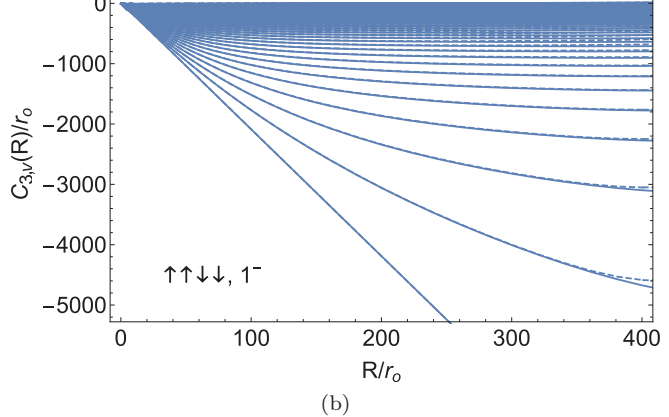
barrier at the unitary limit. For the hyperradial potentials that go to the modified barrier at infinite scattering length (solid curves), the long-range deviation can be represented graphically by plotting $C_{3,\nu}(R) = R[(2\mu/\hbar^2)R^2U_{\nu}(R) - l_{\nu}(l_{\nu}+1)]$, which is based on Eq. (7). Plots of the function $C_{3,\nu}(R)$ for the lowest hyperradial potential for the three symmetries in the three- and four-body systems are shown in Fig. 5.

In Fig. 5, there are numerous curves plotted as a function of R/r_0 that go to a constant at $R/r_0 \to \infty$. Each curve, going from top to bottom, represents a different s-wave scattering length going from $|a_s| = 0$ to $|a_s| \to \infty$. The curve $C_{3,\nu}(R)$ for $|a_s| \to \infty$ is linear due to the shift in $l_{\rm eff}$ at the unitary limit. A similar behavior in the function $C_{3,\nu}(R)$ is observed in the other hyperradial channels and symmetries not shown in Fig. 5. The universal constant for each system and symmetry is determined through performing fitting procedures to the curves shown in Figs. 4 and 5. From this curve-fitting procedure, where each curve is fit to an inverse power law of varying order, the universal constant C_{ν} for the lowest Born-Oppenheimer potential, along with the reduced angular momentum quantum number l_u , is extracted. In Figs. 6(a)-6(c), plots of $C_{3,1}/r_0$ versus a_s/r_0 for a single Gaussian two-body interaction are shown for the three different N-body systems with Figs. 6(a)-6(c) representing the $\uparrow \uparrow \downarrow$, $\uparrow \uparrow \downarrow \downarrow$, and ↑↑↑↓ spin configurations, respectively. In each panel, results are given for the three natural parity symmetries 0⁺ as circles, 1⁻ as squares, and 2⁺ as diamonds. The behavior of the dependence of $C_{3,1}$ on the scattering length is linear for large values of $|a_s/r_0|$; thus, through fitting a linear function to the data shown in Figs. 6(a)-6(c) for the lowest hyperradial channel and for the higher hyperradial channels (not shown), the universal parameters C_{ν} are extracted from the slope of the fit and given in Table II.

Universality in the hyperradial potentials at long range appears for continuum states as a reduction in the angular momentum barrier at infinite scattering length. This is further supported in Fig. 7, which shows a plot of $C_3(R)$ for the lowest hyperradial potential using different two-body interactions. The two-body interactions used in Fig. 7 are of the form given by Eq. (5a). At large hyperradius, the hyperradial potentials collapse onto one curve, demonstrating long-range universality in these continuum states. Only at small hyperradii, at distances less than $R/r_0 \sim 20$, does the short-range nature of the two-body interaction become important and nonuniversal behavior emerges. The analysis of the long-range behavior of the hyperradial potentials thus far has been for the individual spin components of the interacting fermions.

In other systems, such as the few-nucleon systems in nuclear physics, the good quantum numbers are either the total orbital angular momentum and spin L^{π} and S, or the total angular momentum J^{π} in an LS coupling scheme. For the three-body system, the symmetries treated are $(L^{\pi}, S) = (0^+, 1/2)$ and $(1^-, 1/2)$. Likewise, for the four-body system, the symmetries treated are $(L^{\pi}, S) = (0^+, 0)$ and $(1^-, 0)$. From the nuclear studies, near-unitary physics was explored for both three-body and four-body systems in the symmetries $(L^{\pi}, S) = (1^-, 1/2)$ and $(0^+, 0)$, respectively. The long-range universal behavior addressed above manifests itself in fewneutron systems as a result of the large neutron-neutron singlet





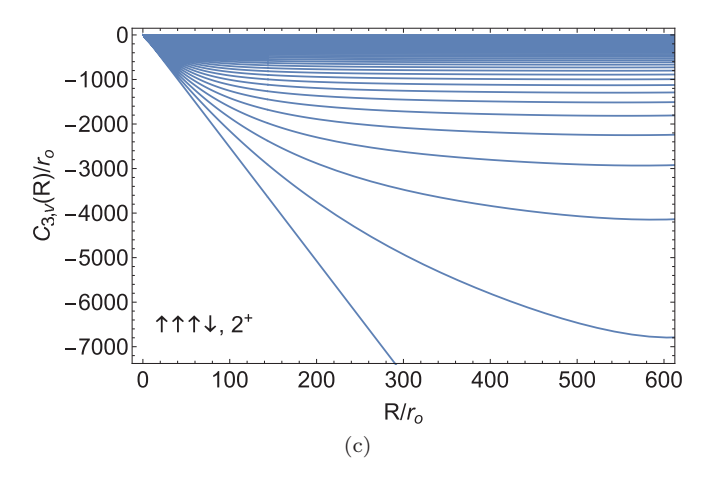


FIG. 5. The lowest few Born-Oppenheimer potential curves for (a) the $(\uparrow\uparrow\downarrow\downarrow)$ equal-mass three-body system for the 0^+ symmetry, (b) the $(\uparrow\uparrow\downarrow\downarrow)$ equal-mass four-body system for the 1^- symmetry, and (c) the $(\uparrow\uparrow\uparrow\downarrow\downarrow)$ equal-mass four-body system for the 2^+ symmetry. The strength of the two-body interactions between all particles is rescaled from the noninteracting limit up to the *s*-wave unitary limit $(a_s \to -\infty)$. From highest to lowest, the highest curve is the noninteracting case, the lowest curve is the *s*-wave unitary case, and a curve in between is for a finite *s*-wave scattering length. The solid curves are for the adiabatic potential and the dashed curves include the second-derivative nonadiabatic correction. The hyperradius has been rescaled by the range of the Gaussian interaction r_0 . The curves for the other symmetries are qualitatively similar and not shown here.

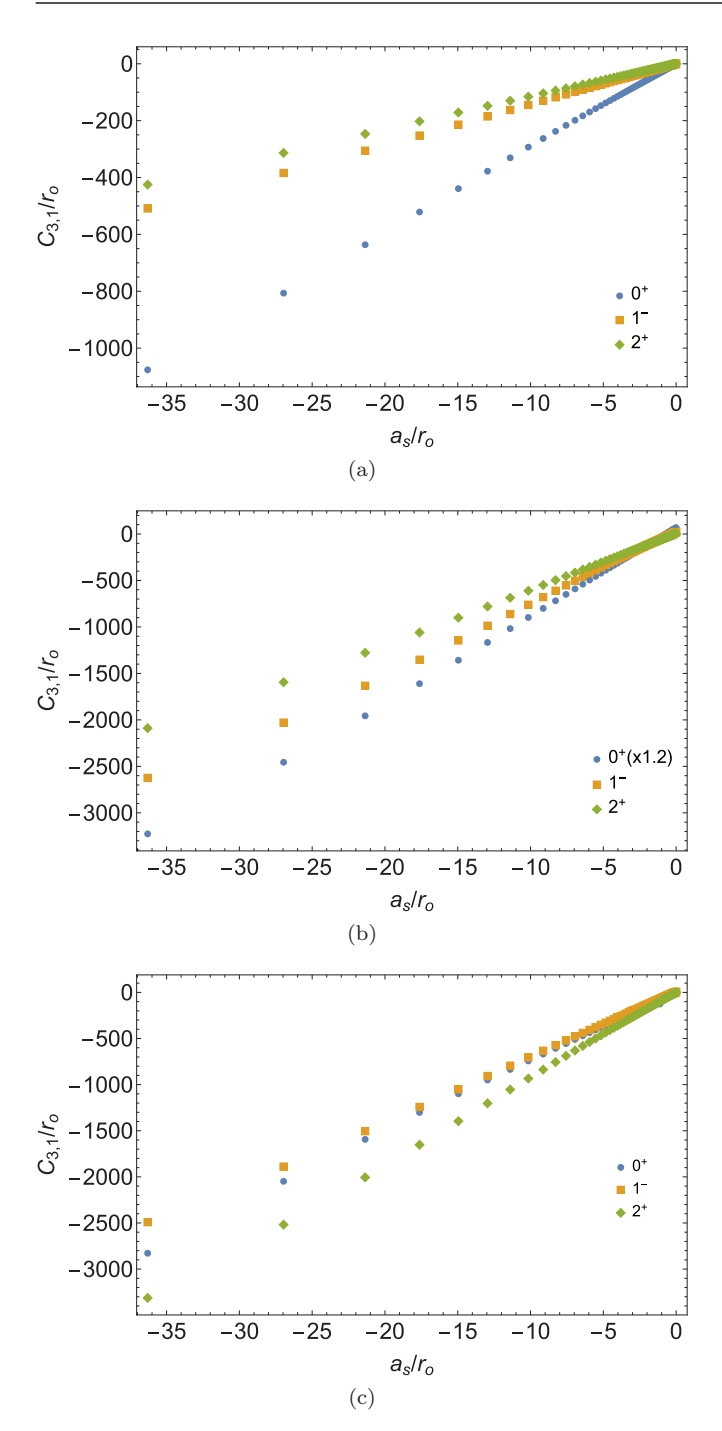


FIG. 6. The long-range coefficient $C_{3,1}/r_0$ versus a_s/r_0 in the lowest Born-Oppenheimer potential for the (a) $(\uparrow\uparrow\downarrow)$, (b) $(\uparrow\uparrow\downarrow\downarrow)$, and (c) $(\uparrow\uparrow\uparrow\downarrow)$ equal-mass systems for the symmetries $L^{\pi}=0^+$ (circles), 1^- (squares), and 2^+ (diamonds). For values of the s-wave scattering length near the unitary limit ($|a_s/r_0| > 10$), $C_{3,\nu}$ grows in proportion to a_s , in accordance with Eq. (7). These results are for a single Gaussian two-body interaction of width r_0 . The data for the other hyperspherical channels yield qualitatively similar results to the lowest channel in each symmetry, and thus are not shown here.

two-body s-wave scattering length. This behavior has been studied for the three- and four-interacting-neutron systems [15,16]. Through spin recoupling, the long-range $1/R^3$ coefficients for a given total spin S in the lowest hyperradial channel

can be determined from the values given in Table II. Some results for the total spin states are given in Table III for three-and four-body systems. The long-range coefficient for given total spin S is typically not relevant for cold-atom systems in the presence of a magnetic field since S is not a good quantum number in this case.

In nuclear physics, there is a classification of spin-1/2 particles interacting in the unitarity regime denoted as "unparticles" that can be described from conformal field theory [42,43]. An example of such systems are clusters of neutrons. The energy dependence of the differential cross section for an N-body system is given as $d\sigma/dE \propto E^{\Delta-5/2}$, where Δ is the conformal dimension for the N-body system. Rewriting the energy dependence in terms of the wave number k, one can see that from the Wigner threshold law where $d\sigma/dE \propto k^{2l_{\rm eff}+1}$, Δ and $l_{\rm eff}$ are related through the expression $\Delta = l_{\rm eff} + 3$. Using the values of l_u given in Table III, the conformal dimensions given in Ref. [43] are reproduced for the N=3, 4 cases.

C. Low-energy behavior of elastic phase shifts

The long-range behavior of the Born-Oppenheimer potentials discussed in the previous section leads to important implications at low collision energies. As described, for the long-range behavior of the adiabatic potentials for s-wave two-body interactions near the unitary limit, specifically near the first s-wave pole in a_s , the adiabatic potentials exhibit a $1/R^3$ long-range tail proportional to the scattering length a_s , represented by Eq. (7). Using the Born approximation, the low-energy elastic N-body scattering phase shift for a given angular momentum $l_{\rm eff}$ is

$$\delta_{l_{\text{eff}}}(k) = -[C/(2l_{\text{eff}}(l_{\text{eff}} + 1))]k,$$
 (8)

where C is the coefficient of the $1/R^3$ term in Eq. (7). Moreover, as was mentioned above, the squared S-matrix element for recombination is proportional to $k^{2l_{\text{eff}}+1}$ in the generalized Wigner threshold law for that process [44,45], when starting from an initial channel with centrifugal potential barrier coefficient $l_{\text{eff}}(l_{\text{eff}}+1)$.

Figure 8 shows a sampling of elastic phase shifts for a Gaussian two-body interaction for different scattering lengths. The four-body elastic phase shift is given as a function of the wave number k for different negative s-wave scattering lengths to highlight the changes in the low-energy behavior as the scattering length increases from zero to the unitary limit. Also shown in Fig. 8 is the low-energy limit derived from the first Born approximation, represented by the black dashed lines. The implications of this linear behavior of the phase shift with wave number comes into the density of final continuum states, defined through the energy derivative of the phase shift for a single-channel calculation or through the time-delay matrix in a multichannel calculation. From Eq. (8), the low energy density of states, related through d/dE, results in an energy enhancement near threshold of 1/E.

TABLE II. Long-range coefficients for the three- and four-body equal-mass systems in the lowest few hyperradial channels for different symmetries. The columns specify the symmetry L^{π} , the hyperspherical channel index ν corresponding to a channel that gives a reduced value of l_{eff} at unitarity, the noninteracting (l_{eff}) and unitary (l_u) angular momentum quantum numbers, and the universal $1/R^3$ coefficient C_{ν} . The label l_u^{ref} indicates the value of l_u extracted from various references. The error bars are estimated based on convergence of the basis used and on curve fitting at large R.

L^{π}	ν	$l_{ m eff}$	l_u	$l_u^{ m ref}$	$C_{ u}$
			(a) (↑↑↓) system		
0^+	1	7/2	1.668(2)	1.6662 ^a , 1.682 ^b	29.47(5)
	2	11/2	4.628(2)	4.6274 ^a	43.37(5)
	3	15/2	6.616(2)	6.6145 ^a	62.3(5)
	5	19/2	8.338(5)	8.3323 ^a	147(5)
1-	1	5/2	1.273(2)	1.2727 ^a , 1.275 ^b	14.19(5)
	2	9/2	3.859(2)	3.85825 ^a	14.63(5)
	4	13/2	5.217(2)	5.21643 ^a	74.91(5)
	7	17/2	7.556(5)	7.553 ^a	98.4(5)
2+	1	7/2	2.605(2)	2.60498 ^a	11.56(5)
	2	11/2	4.296(2)	4.29541 ^a	54.68(5)
	5	15/2	6.734(2)	6.73883 ^a	40.52(5)
	9	19/2	8.340(5)	8.3371 ^a	136.5(5)
			(b) $(\uparrow \uparrow \downarrow \downarrow)$ system		
0^{+}	1	5	2.02(2)	2.028^{c}	72.0(3)
	2	7	4.45(5)	4.441 ^d	138(2)
	3	7	5.03(2)	5.029 ^d	77.0(5)
	4	7	5.36(2)	5.348 ^d	59.6(5)
1-	1	6	4.11(2)	4.0978 ^d	73.7(3)
	2	6	4.18(2)	4.1758 ^d	46.1(3)
	3	6	4.75(2)	4.7305 ^d	45(2)
	4	8	5.73(5)	5.669 ^d	141(2)
2+	1	5	2.95(2)	2.9185 ^d	59.0(3)
	2	7	4.54(2)	4.539 ^d	114(2)
	3	7	5.04(2)	5.039 ^d	96.3(5)
	4	7	5.64(2)	5.6288 ^d	64.1(5)
			(c) (↑↑↑↓) system		,
0^{+}	1	7	5.35(2)	5.3466(1) ^e	75.8(3)
	2	9	6.88(2)	6.8637^{d}	134(2)
	3	9	7.85(2)	7.8409 ^d	98(1)
	4	9	8.35(2)	8.3484 ^d	36(2)
1-	1	6	4.17(2)	4.1770 ^d	69.3(3)
	2	6	4.73(1)	4.7300^{d}	45.2(5)
	3	8	5.81(2)	5.8068 ^d	125(3)
	4	8	6.75(3)	6.7219 ^d	92.2(5)
2+	1	7	5.03(2)	5.0385 ^d	92.2(5)
	2	7	5.74(2)	5.7208 ^d	60.8(5)
	3	7	5.94(2)	5.9242 ^d	40.2(5)
	5	9	7.31(2)	7.2742 ^d	131(3)

^aReference [7].

IV. INTERACTING FERMIONS AT THE *P*-WAVE UNITARY LIMIT

The second type of few-body fermionic systems looked at in this study are the interactions of identical spin-polarized fermions, which interact through p-wave interactions. The focus of this study is to understand four-body properties for these systems and relate them to the corresponding three-body properties, which have been studied in past theoretical

and experimental works [10,11,13,46–49]. In spin-polarized fermionic systems at unitarity, it has been shown in a number of studies that there is no Efimov effect that emerges at unitarity, unlike for bosonic systems [13,50–52]. Short-range effects on three- and four-body properties are investigated for the spin-polarized configuration in the 1^- and 0^+ symmetries, respectively. Through solving the full Schrödinger equation over all space, the three-body binding energy is obtained as a function of the p-wave scattering volume for

^bReference [6].

^cReference [39].

^dReference [40].

^eReference [41].

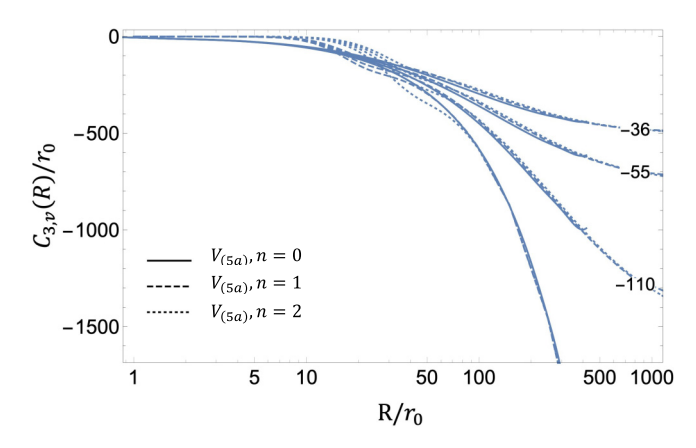
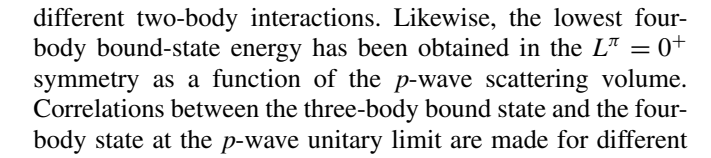


FIG. 7. A comparison of the long-range coefficient $C_{3,1}$ versus a_s in the lowest Born-Oppenheimer potential for the $(\uparrow \uparrow \downarrow)$ equal-mass three-body system shown for three different two-body interactions given in Eqs. (5). The parameters for the interactions are given in Table I for s waves. The coefficient $C_{3,1}$ and the hyperradius R are rescaled by the range of the single Gaussian interaction r_0 . The set of three curves is labeled by the ratio of a_s/r_0 shown on the right-hand side. Universality kicks in for large hyperradius, as indicated by the different interactions converging to one curve for each scattering length.



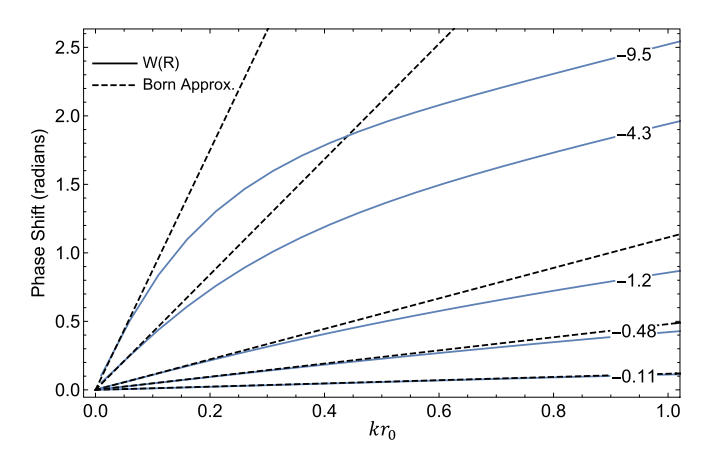


FIG. 8. Single-channel elastic phase shifts for collisions in the lowest hyperspherical continuum channel. Each curve is computed using a different two-body s-wave scattering length, where the ratio a_s/r_0 is given for a Gaussian interaction and displayed on the right. The low-energy behavior is governed by the characteristics of the long-range form of the hyperradial potential [see Eq. (7)]. The $1/R^3$ term in the long-range form gives rise to a linear dependence on wave number k of the phase shift, in accordance with the Wigner threshold law. This linear dependence, derived using the Born approximation in Eq. (8), is shown as the black dashed lines.

two-body interactions. The results are presented in a Tjon plot, similar to ones shown for bosonic systems in past publications [27,51–54], and are shown in Fig. 9.

Figure 9 is a Tjon plot that shows the correlation between the three-body trimer energy in the 1⁻ symmetry and the

TABLE III. Long-range coefficients for the three-body system with total angular momentum and parity L^{π} , and total spin S. For each L and S, the noninteracting angular momentum quantum number l_{eff} is given along with the reduced value l_u at the s-wave unitary limit. The last column gives the numerical results for the scattering-length-dependent coefficient C_{ν} from Eq. (7) for the hyperspherical channel ν that gives a reduced l_{eff} at unitarity. The error bars are estimated based on convergence of the basis used and on curve fitting at large R.

N	(L^{π},S)	ν	$l_{ m eff}$	l_u	l_u^{ref}	$\mathcal{C}_{ u}$
3	(1-, 1/2)	1	5/2	1.275(3) ^a	1.2727 ^b	15.1(3) ^a
		2	9/2	3.861(3) ^a	3.8582 ^b	15.2(3) ^a
		3	13/2	5.219(3) ^a	5.2164 ^b	77.7(3) ^a
		4	17/2	17/2	17/2	
		5	17/2	$7.555(3)^{a}$	7.553 ^b	108(3) ^a
3	$(0^+, 1/2)$	1	7/2	1.668(5)	1.6662 ^b	29.8(5)
		2	11/2	4.630(5)	4.6274 ^b	44.6(5)
		3	15/2	6.63(2)	6.6145 ^b	63.0(5)
		4	19/2	8.35(2)	8.3323 ^b	156(5)
4	$(0^+, 0)$	1	5	$2.02(2)^{a}$	$2.0094(1)^{c}$	86.7(3) ^a
		2	7	$4.45(2)^{a}$	$4.444(3)^{d}$	156(3) ^a
		3	7	5.07(5) ^a	$5.029(3)^{d}$	61.1(3) ^a
		4	9	$6.97(5)^{a}$	$6.863(3)^{d}$	$209(3)^{a}$
		5	9	$7.26(5)^{a}$	$7.121(3)^{d}$	87.8(3) ^a
4	$(1^-,0)$	1	6	4.11(2)	4.0978 ^e	73.6(5)
		2	8	5.74(5)	5.667 ^e	116(5)
		3	8	6.57(5)	6.505 ^e	81.2(5)

^aValue extracted from Ref. [16]. The C_{ν} coefficients are multiplied by $\sqrt{\mu/\mu'}$, where μ' is the neutron-neutron reduced mass.

^bReference [7].

^cReference [39].

dReference [41].

eReference [40].

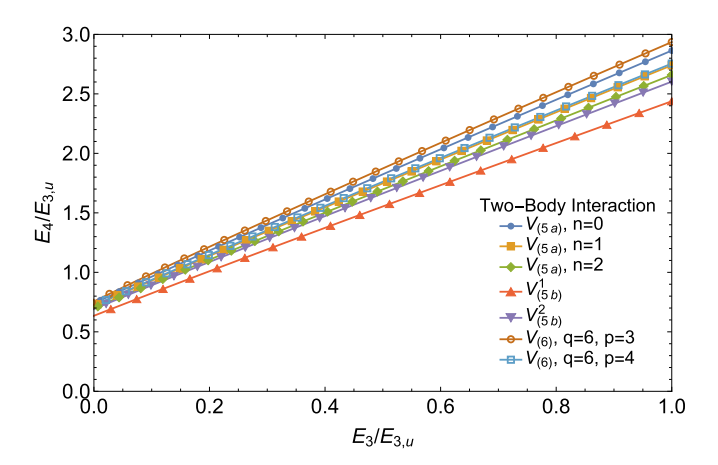


FIG. 9. A Tjon plot of the correlation between the universal three-body binding energy in the $L^{\pi}=1^{-}$ and the lowest four-body binding energy in the $L^{\pi}=0^{+}$ symmetry. Each point type corresponds to a different two-body interaction, given in the legend and labeled by the equation number. The parameters for the interactions are given in Table I for p waves. The axes are rescaled by the trimer energy at the unitary limit to place all of the data sets on the same scale.

four-body tetramer energy in the 0+ for spin-polarized fermions in each case (i.e., the total spin is S = 3/2 and S = 2 for the three- and four-body systems, respectively). From Fig. 9, the three- and four-body ground-state energies are given for different two-body interactions, provided in Eqs. (5) and (6). The respective three-body and four-body energies are rescaled by the trimer value at the p-wave unitary limit in order to display the results from each interaction on the same scale. The correlation between the trimer and tetramer energies is linear for each interaction type. A linear fit was performed over the average of the two-body interaction models to determine an effective correlation between the trimer and tetramer states. The linear fit parameters are given in the figure and the correlation has been determined (with an *R*-squared value of 0.9754) to be $E_4^{0^+} = 2.024(11)E_3^{1^-} + 0.718(6)E_{3,u}^{1^-}$, where $E_4^{0^+}$ is the tetramer energy for $L^{\pi} =$ 0^+ , $E_3^{1^-}$ is the trimer energy for $L^{\pi} = 1^-$, and $E_{3\mu}^{1^-}$ is the trimer energy at the p-wave unitary limit. There is a similar relationship between the trimer and tetramer states in four-boson systems at the s-wave unitary limit, in relation to the Efimov effect. In the bosonic systems, there exist two tetramer bound states for every hyperspherical potential describing the two-body fragmentation to an Efimov trimer + free particle [18,23,55]. The relationship between the two universal tetramers and the corresponding Efimov trimer at unitarity was determined to be $E_{4B}^{\hat{n},m} = c_m E_{3B}^n$, where $c_1 =$ 4.58 and $c_2 = 1.01$, as described in Eq. (2) of Ref. [18]. Using momentum-space transition operators to study these universal tetramers for unitary bosons, Deltuva computed the universal coefficients to be $c_1 = 4.610(1)$ and $c_2 = 1.00227(1)$ [55]. In the case of fermions, the scaling coefficient of the trimer energy is smaller than the scaling factor of the ground state for bosons by almost a factor of 2. This difference can be interpreted as resulting from the Pauli repulsion effects seen in fermionic systems that are absent from bosonic systems.

TABLE IV. Energy and scattering volume ratios at the p-wave unitary limit for the spin-polarized $(\uparrow\uparrow\uparrow\uparrow)$ system in the 0^+ symmetry. Each column represents a different two-body interaction from Eqs. (5) and (6), where the parameters are given in Table I for p waves. Each row labels the ratio between four- and three-body properties, where row 1 gives the ratio of the 0^+ tetramer energy to the 1^- trimer energy at unitarity, row 2 gives the ratio of overall scaling factors $(\beta_{p,4}^{0^+}/\beta_{p,3}^{1^-})$ of the two-body interaction [i.e., $V'(r) = \beta V(r)$] needed to bind the trimer and tetramer, and row 3 gives the ratio of effective p-wave scattering lengths $a_p = V_p^{1/3}$ at which tetramer and trimer states first form at zero energy.

V_{ij}	$V_{(5a)}^{n=0}$	$V_{(5a)}^{n=1}$	$V_{(5a)}^{n=2}$	$V_{(5b)}^{(1)}$	$V_{(5b)}^{(2)}$	$V_{(6)}^{p=3}$	$V_{(6)}^{p=4}$
$E_{4,u}^{0^+}/E_{3,u}^{1^-}$	2.864	2.740	2.659	2.603	2.446	2.936	2.755
$eta_{p,4}^{0^+}/eta_{p,3}^{1^-}$	0.935	0.941	0.944	0.944	0.953	0.933	0.938
$a_{p,4}^{0^+}/a_{p,3}^{1^-}$	0.875	0.874	0.876	0.882	0.874	0.891	0.887

Unlike the four-boson case, the four-fermion tetramer is not universal; i.e., its energy depends on the short-range interaction. Table IV shows this ratio for different two-body interactions. The reason for this nonuniversal behavior is similar to that in the four-boson case for the two tetramers in the lowest hyperradial potentials in Ref. [18]. The hyperradial potentials that support the ground-state tetramers in the fermion case have potential minima on the order of the range of the interaction. Thus, the mean distance between any two fermions in the tetramer is of the order of the two-body interaction range, so it stands to reason that the trimer and tetramer energies will vary depending on the short-range behavior of the interaction, similar to that found in the lowest hyperradial potential for the boson case.

Other quantities of interest are the points at which the trimer and tetramer states transition from being a resonance in the continuum to being a bound state. These transition points are characterized by the ratio of the effective p-wave scattering lengths, $a_p = V_p^{1/3}$, at which this transition occurs for the three- and four-body systems. This ratio is numerically determined here through a full diagonalization of the Hamiltonian for the different two-body interactions used to characterize the energy ratio and is shown in the second row of Table IV. From these results, the ratio $a_{p,4}^{0^+}/a_{p,3}^{1^-} \sim 0.88$ is a universal quantity, as it is found to be insensitive to the short-range behavior of the interaction, with a standard deviation of 0.01, i.e., 1.0% of the mean.

The quantity $a_{p,4}/a_{p,3}$ has importance for four-body recombination processes. In this case, the relevant recombination process is $A+A+A+A \leftrightarrow A_3+A$ for $L^\pi=0^+$, where A is a fermion. Given the two-body p-wave scattering volume $V_{p,3}^{AA}$, with $a_{p,3}=[V_{p,3}^{AA}]^{1/3}$, where the A_3 trimer transitions from resonant to bound, there will be an enhancement in the four-body recombination for an ultracold gas into deep dimers or trimers at scattering volumes $V_{p,4}^{AA}$, with $a_{p,4}=[V_{p,4}^{AA}]^{1/3}$, where the tetramer A_4 transitions from resonant to bound. The ratio $a_{p,4}^{0^+}/a_{p,3}^{1^-}$ is universal with small deviations (two standard deviations of the mean, or $\sim 2\%$) due to short-range effects (see Table IV). The location of the enhancement in the four-body recombination process where

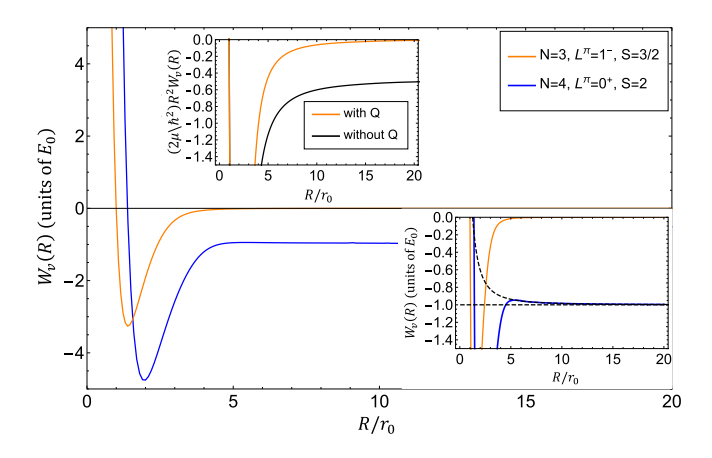


FIG. 10. Lowest hyperradial potentials for the three- and four-identical fermionic systems in the spin-polarized state at the p-wave unitary limit. The lower inset plot shows these potentials on a smaller energy scale to highlight the asymptotic behavior of the lowest four-body potential at large hyperradius. The dashed lines show the expected asymptotic behavior as the potential approaches the trimer + free particle threshold. The upper inset plot shows the three-body potential rescaled by R^2 with and without the second-derivative nonadiabatic coupling. This highlights the long-range behavior, specifically showing the negative, nonzero coefficient of R^{-2} without the diagonal coupling added, indicating Efimov physics. However, this is not a true Efimov feature, as this coefficient vanishes after including the nonadiabatic coupling.

the four-body state becomes resonant with the continuum is governed by $a_{p,3}$ of the system and should be found in the range $0.87a_{p,3}^{1-} < a_{p,4}^{0+} < 0.89a_{p,3}^{1-}$ or, in terms of the *p*-wave scattering volume, $0.66V_{p,3}^{1-} < V_{p,4}^{0+} < 0.70V_{p,3}^{1-}$. It should be noted that the small deviations resulting from short-range effects are of the same order of magnitude as those found in the *N*-boson case when looking at the lowest Efimov states [25,26,56].

These identical fermionic systems interacting at the *p*-wave unitary limit are further studied by calculating the adiabatic potential curves as functions of the hyperradius. To verify the relation between the trimer energy and tetramer energy given in Table IV, the lowest few hyperradial potential curves for the spin-polarized (S = 3/2 and S = 2) three- and four-body systems were computed, along with the diagonal nonadiabatic second-derivative correction to provide an upper and lower bound to these binding energies. Figure 10 shows the lowest three- and four-body hyperradial potential with the diagonal nonadiabatic correction. In Fig. 10, the lowest effective hyperradial potentials for the three- and four-identical fermionic spin-polarized systems are shown in the range $0 < R/r_0 < 20$. The two inset plots highlight some features of these effective potentials at large hyperradius related to fragmentation pathways and the Efimov effect. The inset plot on the lower left shows a zoomed-in view of the main figure which highlights the asymptotic behavior of the lowest 0⁺ four-body potential. This inset shows the behavior of the lowest four-body potential at large hyperradius, which represents the two-body fragmentation of the four-body system into the universal trimer in the 1⁻ state plus a free particle with a relative angular momentum quantum number of l = 1.

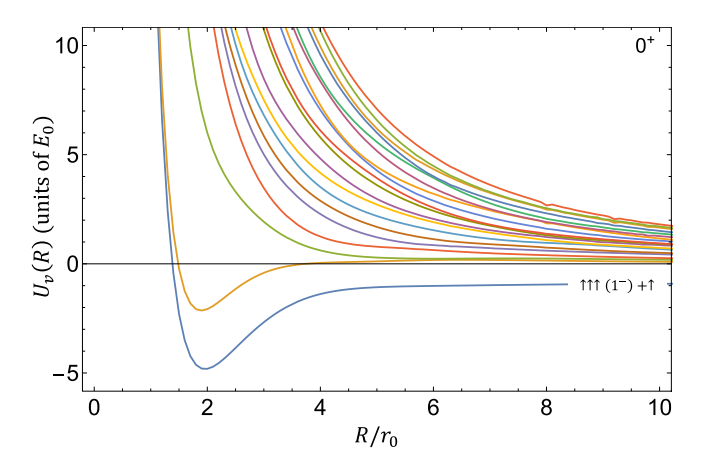


FIG. 11. The hyperradial potentials for the four-fermion system in the $(\uparrow\uparrow\uparrow\uparrow)$ spin configuration. Each curve represents a different hyperradial potential with channel index ν that increases from the lowest to highest curve. The two-body interaction between $(\uparrow\uparrow)$ spins is set to the first p-wave unitary limit. For this set of two-body interactions, there is one two-body breakup threshold below the four-body continuum, labeled by the fragmentation of the spins and the angular momentum of the trimer.

This is further emphasized by the comparison of the effective potential with a purely centrifugal barrier (represented by the dashed line) with l=1. The horizontal dashed line shows the trimer energy, which aligns with the position of the trimer energy in the well of the three-body potential in the main figure.

The second inset shows the lowest three-body hyperradial potential multiplied by R^2 with and without the second-derivative nonadiabatic coupling term. As shown, the Born-Oppenheimer potential falls off as $1/R^2$ with a negative power of approximately -0.5 [i.e., $U_0(R) \rightarrow -\frac{\hbar^2}{4\mu R^2}$]. From this attractive long-range behavior, the lowest three-body adiabatic potential behaves like the Efimov potential manifested in the three-boson system at s-wave unitarity, which has the form $U_0(R) = -\frac{\hbar^2}{2\mu R^2}(s_0^2 + 1/4)$ with $s_0 = 1.0061$. Comparing the $1/R^2$ coefficient for bosons with the coefficient of the adiabatic potential for three fermions, the value of the Efimov parameter is $s_0 \approx 0.5$. Since the value of s_0 is greater than zero, this would indicate an Efimov-like effect in this fermionic system. However, it has been determined that no such Efimov effect actually exists in these systems. The nonadiabatic second-derivative coupling exactly cancels this attractive $1/R^2$ term in the adiabatic potential, indicated by the upper line in the inset that goes to zero at large R. This indicates that the lowest effective three-body hyperradial potential does not have an Efimov-like behavior at large hyperradius which would lead to an infinite set of bound trimer states.

Further evidence for the nonexistence of the Efimov effect for three identical spin-polarized fermions is shown in the hyperradial mapping of the four-body case, shown in Fig. 11. The spectrum of hyperradial potentials in the four-body case gives further insights into the interactions of identical fermions at unitarity. From Fig. 11, there is only one fragmentation pathway of the four-body system to a two-body system

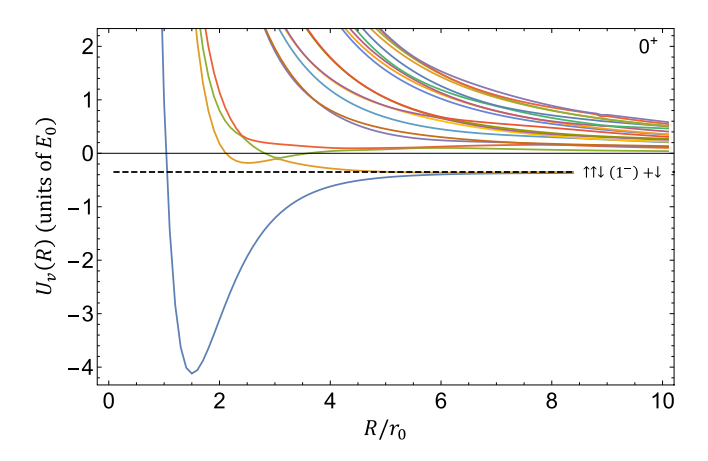


FIG. 12. The Born-Oppenheimer potentials for the four-fermion system in the $(\uparrow\uparrow\downarrow\downarrow)$ spin configuration. Each curve represents a different hyperradial potential with channel index ν that increases from the lowest to highest curve. The two-body interaction between $(\uparrow\uparrow)$ spins is set to the first p-wave unitary limit, while the $(\uparrow\downarrow)$ is set to the first s-wave unitary limit. For this set of two-body interactions, there is one two-body breakup threshold below the four-body continuum threshold, labeled by the fragmentation of the spins and the angular momentum of the trimer.

representing the fragmentation into a *p*-wave universal trimer and a free particle, shown in the lowest potential. If there were a three-body Efimov effect in the identical spin-polarized fermion case, then there should be an infinite number of hyperradial potentials, each one going to one of the Efimov trimers as is the case of bosonic systems [18].

There are other interesting features in the spectrum of the four-body system at the p-wave unitary limit that should be noted. One of the main features, as described earlier, is the presence of a bound tetramer state in the lowest hyperspherical potential. In the $L^{\pi}=0^+$ symmetry, there is a single tetramer bound state in the lowest potential which asymptotically, at large hyperradius, goes to the trimer plus free particle energy threshold. The binding energy of the spin-polarized tetramer is related to the corresponding trimer energy through a relation described by a Tjon plot like the one shown in Fig. 9. There is also a hyperradial potential representing the second hyperradial eigenvalue of the adiabatic Hamiltonian in Eq. (2) that exhibits a potential minimum below E=0 which has the potential to contain either bound or resonant states.

Next, the hyperradial potentials are mapped out for the $(\uparrow\uparrow\downarrow\downarrow)$ and $(\uparrow\uparrow\uparrow\downarrow)$ spin configurations for total orbital angular momentum $L^{\pi}=0^+$. The lowest few hyperradial potentials for the $(\uparrow\uparrow\downarrow\downarrow)$ configuration are shown in Fig. 12. In this spin configuration and symmetry, the lowest two hyperradial potentials converge to a two-body breakup threshold below zero energy that represents the two-body breakup into a trimer plus a free particle in the spin configurations $\uparrow\uparrow\downarrow(1^-)+\downarrow$ and $\downarrow\downarrow\uparrow(1^-)+\uparrow$, where the trimer state is labeled by its total orbital angular momentum, which is 1^- . Through angular momentum coupling, the relative angular momentum between the trimer and free particle in the 0^+ symmetry is $l_{\rm rel}=1$. In this spin configuration, the lowest

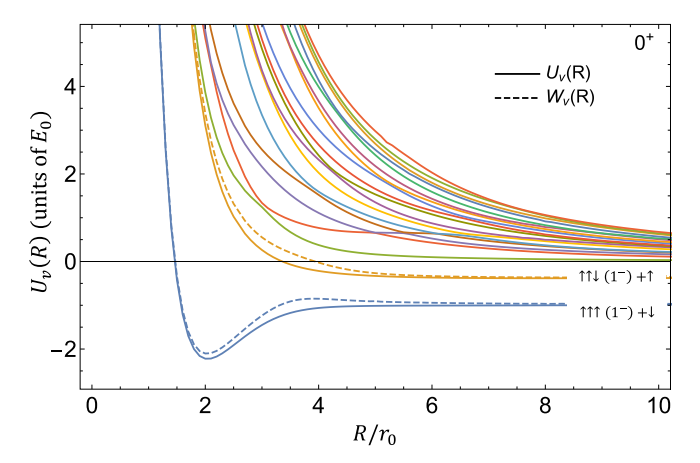


FIG. 13. The hyperradial potentials for the four-fermion system in the $(\uparrow\uparrow\uparrow\downarrow)$ spin configuration. Each curve represents a different hyperradial potential with channel index ν that increases from the lowest to highest curve. The two-body interaction between $(\uparrow\uparrow)$ spins is set to the first p-wave unitary limit, while the $(\uparrow\downarrow)$ is set to the first s-wave unitary limit. For this set of two-body interactions, there are two two-body breakup thresholds below the four-body continuum, labeled by the fragmentation of the spins and the angular momentum of the trimer. The solid curves are the Born-Oppenheimer potentials and the dashed curves are the effective hyperradial potentials that include the diagonal nonadiabatic second-derivative coupling.

hyperradial potential supports one tetramer bound state in the 0^+ symmetry.

For the other spin configuration, $(\uparrow\uparrow\uparrow\downarrow)$, the hyperradial potentials are shown in Fig. 13. In this spin configuration and symmetry, the lowest two hyperradial potentials converge to two-body breakup thresholds below zero energy that represents the two-body breakup into a trimer plus a free particle in the spin configurations $\uparrow\uparrow\downarrow(1^-)+\uparrow$ and $\uparrow\uparrow\uparrow(1^-)+\downarrow$, where again the trimers are in the 1^- symmetry. In this spin configuration, the hyperradial potentials do not support a tetramer state in this symmetry. In summary, for total orbital angular momentum 0^+ , the spin configurations that support tetramer bound states are the $(\uparrow\uparrow\downarrow\downarrow)$ and $(\uparrow\uparrow\uparrow\uparrow)$ configurations where the $(\uparrow\downarrow)$ interactions are tuned to the *s*-wave unitary limit and the $(\uparrow\uparrow)$ and $(\downarrow\downarrow)$ interactions are tuned to the *p*-wave unitary limit.

V. CONCLUSIONS

In this work, the three- and four-body fermionic systems are studied for various equal-mass cases, interacting near their s-wave and/or p-wave unitary regimes. Specifically, this work focuses on the regime where there are no two-body bound states (i.e., near the first s-wave pole in a_s and the first p-wave pole in V_p). The symmetries treated in this work are $L^{\pi} = 0^+, 1^-,$ and 2^+ in the spin configurations $(\uparrow \uparrow \downarrow)$ for the three-body system and $(\uparrow \uparrow \downarrow \downarrow), (\uparrow \uparrow \uparrow \downarrow),$ and $(\uparrow \uparrow \uparrow \uparrow)$ for the four-body system. In the first part of this work, the systems considered reside near the s-wave unitary limit; our analysis treats universal properties of the hyperradial potentials and the resultant effects on the low-energy elastic phase shifts for continuum scattering. At infinite scattering length, there

is a modification to the angular momentum barrier in some of the continuum hyperradial potentials. This modification is followed by a universal long-range next-order term in the hyperradial potentials that falls off as $1/R^3$ and is proportional to the scattering length and is independent of the short-range details of the two-body interaction, and is thus universal. This universal constant is characterized for different symmetries of several three- and four-body systems in the lowest hyperradial continuum channel. As a result of this long-range universal behavior in the potentials, the low-energy phase shift is proportional to the wave number k, i.e., to \sqrt{E} in the energy. This leads to a $1/\sqrt{E}$ in the energy derivative of the phase shift, which is proportional to the density of states in the continuum.

The second part of this article investigates the interaction of equal-mass fermions at the p-wave unitary limit for four particles in the symmetry $L^{\pi}=0^+$ and its implications as it relates to the properties of the three-body system at s-wave and p-wave unitary limits where the s-wave and p-wave dimer energy is at E=0. For the spin-polarized case, where the spins are in the $(\uparrow\uparrow\uparrow\uparrow)$ configuration and the p-wave interactions are tuned from noninteracting to the unitary regime, the spectrum for the symmetry $L^{\pi}=0^+$ shows one four-body tetramer state supported in the lowest hyperradial potential. From the hyperradial potentials, the potential minimum that

supports the tetramer state is located at a distance comparable to the range of the interaction, which is the reason that the ratio of the tetramer energy to the corresponding trimer energy E_4/E_3 is sensitive to the form of the short-range behavior of the two-body interaction; this is analogous to what was previously documented for the tetramer states in the lowest hyperradial potential for the four-boson case.

A key quantity for four-body recombination is the ratio of effective p-wave scattering lengths associated with occurrence of a zero-energy trimer and tetramer resonance. Through an analysis of Tjon plots for different two-body interactions, this ratio is found to be universal with a value of $a_{p,4}^{0^+}/a_{p,3}^{1^-} \sim 0.88$. This universal property provides a probe for where the loss rate in the four-body recombination process $A + A + A + A \leftrightarrow A_3 + A$ is enhanced due to the formation of a bound tetramer for the 0^+ symmetry.

ACKNOWLEDGMENTS

We would like to thank both Doerte Blume and Yu-Hsin Chen for fruitful discussions. We would further like to extend thanks to Yu-Hsin Chen for providing some three-body calculations to check with our numerical results. This work is supported in part by the National Science Foundation, Grant No. PHY-1912350.

- V. N. Efimov, Weakly bound states of three resonantly interacting particles. Sov. J. Nucl. Phys. 12 (1971).
- [2] V. Efimov, Energy levels of three resonantly interacting particles, Nucl. Phys. A **210**, 157 (1973).
- [3] P. Naidon and S. Endo, Efimov physics: A review, Rep. Prog. Phys. 80, 056001 (2017).
- [4] C. A. Regal and D. S. Jin, Experimental realization of the BCS-BEC crossover with a Fermi gas of atoms, Adv. At. Mol. Opt. Phys. **54**, 1 (2007).
- [5] J. von Stecher and C. H. Greene, Spectrum and Dynamics of the BCS-BEC Crossover from a Few-Body Perspective, Phys. Rev. Lett. 99, 090402 (2007).
- [6] D. Blume, J. Von Stecher, and C. H. Greene, Universal Properties of a Trapped Two-Component Fermi Gas at Unitarity, Phys. Rev. Lett. 99, 233201 (2007).
- [7] F. Werner and Y. Castin, Unitary Quantum Three-Body Problem in a Harmonic Trap, Phys. Rev. Lett. **97**, 150401 (2006).
- [8] S. T. Rittenhouse, J von Stecher, J. P. D'Incao, N. P. Mehta, and C. H. Greene, The hyperspherical four-fermion problem, J. Phys. B: At. Mol. Opt. Phys. 44, 172001 (2011).
- [9] M. Greiner, C. A. Regal, and D. S. Jin, Probing the Excitation Spectrum of a Fermi Gas in the BCS-BEC Crossover Regime, Phys. Rev. Lett. 94, 070403 (2005).
- [10] J. Yoshida, T. Saito, M. Waseem, K. Hattori, and T. Mukaiyama, Scaling Law for Three-Body Collisions of Identical Fermions with *p*-Wave Interactions, Phys. Rev. Lett. **120**, 133401 (2018).
- [11] M. Waseem, J. Yoshida, T. Saito, and T. Mukaiyama, Unitarity-limited behavior of three-body collisions in a *p*-wave interacting Fermi gas, Phys. Rev. A **98**, 020702(R) (2018).

- [12] M. Waseem, J. Yoshida, T. Saito, and T. Mukaiyama, Quantitative analysis of *p*-wave three-body losses via a cascade process, Phys. Rev. A **99**, 052704 (2019).
- [13] Y.-H. Chen and C. H. Greene, Efimov physics implications at p-wave fermionic unitarity, Phys. Rev. A 105, 013308 (2022).
- [14] J. P. D'Incao (private communication)
- [15] M. D. Higgins, C. H. Greene, A. Kievsky, and M. Viviani, Nonresonant Density of States Enhancement at Low Energies for Three or Four Neutrons, Phys. Rev. Lett. 125, 052501 (2020).
- [16] M. D. Higgins, C. H. Greene, A. Kievsky, and M. Viviani, Comprehensive study of the three- and four-neutron systems at low energies, Phys. Rev. C 103, 024004 (2021).
- [17] K. Kisamori, S. Shimoura, H. Miya, S. Michimasa, S. Ota, M. Assie, H. Baba, T. Baba, D. Beaumel, M. Dozono, T. Fujii, N. Fukuda, S. Go, F. Hammache, E. Ideguchi, N. Inabe, M. Itoh, D. Kameda, S. Kawase, T. Kawabata *et al.*, Candidate Resonant Tetraneutron State Populated by the ⁴He(⁸He, ⁸Be) Reaction, Phys. Rev. Lett. **116**, 052501 (2016).
- [18] J. von Stecher, J. P. D'Incao, and C. H. Greene, Signatures of universal four-body phenomena and their relation to the Efimov effect, Nat. Phys. **5**, 417 (2009).
- [19] Y. Wang, W. B. Laing, J. von Stecher, and B. D. Esry, Efimov Physics in Heteronuclear Four-Body Systems, Phys. Rev. Lett. 108, 073201 (2012).
- [20] A. Zenesini, B. Huang, M. Berninger, S. Besler, H.-C. Nägerl, F. Ferlaino, R. Grimm, C. H. Greene, and J. von Stecher, Resonant five-body recombination in an ultracold gas of bosonic atoms, New J. Phys. 15, 043040 (2013).
- [21] B. Bazak, J. Kirscher, S. König, M. P. Valderrama, N. Barnea, and U. van Kolck, Four-Body Scale in Universal Few-Boson Systems, Phys. Rev. Lett. 122, 143001 (2019).

- [22] M. Gattobigio and A. Kievsky, Universality and scaling in the n-body sector of Efimov physics, Phys. Rev. A 90, 012502 (2014).
- [23] L. Platter, H.-W. Hammer, and Ulf-G. Meißner, Four-boson system with short-range interactions, Phys. Rev. A 70, 052101 (2004).
- [24] T. Kraemer, M. Mark, P. Waldburger, J. G. Danzl, C. Chin, B. Engeser, A. D. Lange, K. Pilch, A. Jaakkola, H.-C. Nägerl, and R. Grimm, Evidence for Efimov quantum states in an ultracold gas of caesium atoms, Nature (London) 440, 315 (2006).
- [25] J. von Stecher, Five- and Six-Body Resonances Tied to an Efimov Trimer, Phys. Rev. Lett. **107**, 200402 (2011).
- [26] J. von Stecher, Weakly bound cluster states of Efimov character, J. Phys. B: At. Mol. Opt. Phys. 43, 101002 (2010).
- [27] G. J. Hanna and D. Blume, Energetics and structural properties of three-dimensional bosonic clusters near threshold, Phys. Rev. A 74, 063604 (2006).
- [28] D. Blume and Y. Yan, Generalized Efimov Scenario for Heavy-Light Mixtures, Phys. Rev. Lett. **113**, 213201 (2014).
- [29] K. Varga, Y. Suzuki, and J. Usukura, Global-vector representation of the angular motion of few-particle systems, Few-Body Syst. 24, 81 (1998).
- [30] Y. Suzuki, W. Horiuchi, M. Orabi, and K. Arai, Global-vector representation of the angular motion of few-particle systems II, Few-Body Syst. **42**, 33 (2008).
- [31] J. Mitroy, S. Bubin, W. Horiuchi, Y. Suzuki, L. Adamowicz, W. Cencek, K. Szalewicz, J. Komasa, D. Blume, and K. Varga, Theory and application of explicitly correlated Gaussians, Rev. Mod. Phys. 85, 693 (2013).
- [32] K. M. Daily, R. E. Wooten, and C. H. Greene, Hyperspherical theory of the quantum Hall effect: The role of exceptional degeneracy, Phys. Rev. B 92, 125427 (2015).
- [33] J. Wang, Hyperspherical approach to quantal three-body theory, Ph.D. thesis, University of Colorado, Boulder (2012)
- [34] K. M. Daily, J. von Stecher, and C. H. Greene, Scattering properties of the $2e^-2e^+$ polyelectronic system, Phys. Rev. A **91**, 012512 (2015).
- [35] K. M. Daily, Hyperspherical asymptotics of a system of four charged particles, Few-Body Syst. 56, 809 (2015).
- [36] D. Rakshit and D. Blume, Hyperspherical explicitly correlated Gaussian approach for few-body systems with finite angular momentum, Phys. Rev. A 86, 062513 (2012).
- [37] S. T. Rittenhouse, N. P. Mehta, and C. H. Greene, Green's functions and the adiabatic hyperspherical method, Phys. Rev. A 82, 022706 (2010).
- [38] V. E. Colussi, Ultracold gas theory from the top-down and bottom-up, Ph.D. thesis, University of Colorado, Boulder (2017).
- [39] X. Y. Yin and D. Blume, Trapped unitary two-component Fermi gases with up to ten particles, Phys. Rev. A **92**, 013608 (2015).

- [40] D. Rakshit, K. M. Daily, and D. Blume, Natural and unnatural parity states of small trapped equal-mass two-component Fermi gases at unitarity and fourth-order virial coefficient, Phys. Rev. A 85, 033634 (2012).
- [41] J. von Stecher and C. H. Greene, Correlated Gaussian hyperspherical method for few-body systems, Phys. Rev. A **80**, 022504 (2009).
- [42] H. Georgi, Unparticle Physics, Phys. Rev. Lett. 98, 221601 (2007).
- [43] H.-W. Hammer and D. T. Son, Unnuclear physics: Conformal symmetry in nuclear reactions, Proc. Natl. Acad. Sci. USA 118, e2108716118 (2021).
- [44] A. R. P. Rau, Threshold laws, Comments At. Mol. Phys. 14, 285 (1984).
- [45] H. R. Sadeghpour, J. L. Bohn, M. J. Cavagnero, B. D. Esry, I. I. Fabrikant, J. H. Macek, and A. R. P. Rau, Collisions near threshold in atomic and molecular physics, J. Phys. B: At. Mol. Opt. Phys. 33, R93 (2000).
- [46] H. Suno, B. D. Esry, and C. H. Greene, Three-body recombination of cold fermionic atoms, New J. Phys. 5, 53 (2003).
- [47] J. P. Gaebler, J. T. Stewart, J. L. Bohn, and D. S. Jin, *p*-Wave Feshbach Molecules, Phys. Rev. Lett. **98**, 200403 (2007).
- [48] J. J. Zirbel, K.-K. Ni, S. Ospelkaus, J. P. D'Incao, C. E. Wieman, J. Ye, and D. S. Jin, Collisional Stability of Fermionic Feshbach Molecules, Phys. Rev. Lett. 100, 143201 (2008).
- [49] F. Ç. Top, Y. Margalit, and W. Ketterle, Spin-polarized fermions with *p*-wave interactions, Phys. Rev. A **104**, 043311 (2021).
- [50] E. Braaten, P. Hagen, H.-W. Hammer, and L. Platter, Renormalization in the three-body problem with resonant *p*-wave interactions, Phys. Rev. A **86**, 012711 (2012).
- [51] Y. Yan and D. Blume, Energy and structural properties of *n*-boson clusters attached to three-body Efimov states: Two-body zero-range interactions and the role of the three-body regulator, Phys. Rev. A **92**, 033626 (2015).
- [52] D. Blume, Universal Four-Body States in Heavy-Light Mixtures with a Positive Scattering Length, Phys. Rev. Lett. 109, 230404 (2012).
- [53] D. Blume, Few-boson system with a single impurity: Universal bound states tied to Efimov trimers, Phys. Rev. A 99, 013613 (2019).
- [54] D. Blume, Efimov physics and the three-body parameter for shallow van der Waals potentials, Few-Body Syst. 56, 859 (2015).
- [55] A. Deltuva, Properties of universal bosonic tetramers, Few-Body Syst. **54**, 569 (2013).
- [56] F. Ferlaino, S. Knoop, M. Berninger, W. Harm, J. P. D'Incao, H.-C. Nägerl, and R. Grimm, Evidence for Universal Four-Body States Tied to an Efimov Trimer, Phys. Rev. Lett. 102, 140401 (2009).